Biodegradable and Highly Deformable Temperature Sensors for the Internet of Things

Giovanni A. Salvatore, Jenny Sülzle, Filippo Dalla Valle, Giuseppe Cantarella, Francesco Robotti, Petar Jokic, Stefan Knobelspies, Alwin Daus, Lars Büthe, Luisa Petti, Norbert Kirchgessner, Raoul Hopf, Michele Magno, and Gerhard Tröster*

Recent advances in biomaterials, thin film processing, and nanofabrication offer the opportunity to design electronics with novel and unique capabilities, including high mechanical stability and biodegradation, which are relevant in medical implants, environmental sensors, and wearable and disposable devices. Combining reliable electrical performance with high mechanical deformation and chemical degradation remains still challenging. This work reports temperature sensors whose material composition enables full biodegradation while the layout and ultrathin format ensure a response time of 10 ms and stable operation demonstrated by a resistance variation of less than 0.7% when the devices are crumpled, folded, and stretched up to 10%. Magnesium microstructures are encapsulated by a compostable-certified flexible polymer which exhibits small swelling rate and a Young's modulus of about 500 MPa which approximates that of muscles and cartilage. The extension of the design from a single sensor to an array and its integration onto a fluidic device, made of the same polymer, provides routes for a smart biodegradable system for flow mapping. Proper packaging of the sensors tunes the dissolution dynamics to a few days in water while the connection to a Bluetooth module demonstrates wireless operation with 200 mK resolution prospecting application in food tracking and in medical postsurgery monitoring.

1. Introduction

Biodegradable, compostable, and dissolvable materials are, today more than ever, at the attention of scientists and public audience for the problems linked to food quality, climate change, and waste recyclability.[1,2] Nowadays, thanks to the progress in synthetic chemistry and engineering, chemical properties can be tailored to specific applications. Materials that undergo degradation by biological and/or chemical processes are used for food packaging,[1,3] drug delivery,[4,5] tissue engineering,[4,6] microfluidics,[7] medical tools, and implantable devices.[8,9] Till very recently, electronics have not been on such development path. Degradable forms of electronics, i.e., devices that work for a prescribed time and then disappear via hydrolysis or biochemical reactions, could add intelligence and increase the functionalities of the above-listed systems. Resorbable smart implants constitute the most appealing application but other opportunities exist in security systems, fieldable environmental sensors, food monitoring, and consumer electronics to alleviate the problems inherent to electronic waste. From polymers, the palette of materials has expanded to include organic[10,11] and inorganic semiconductors,[12–14] dielectrics,[15,16] and metals[17] providing all the key ingredients for high-performance electronics.[18] Novel assembly schemes, i.e., printing, have complemented more conventional microtechnology techniques and enabled the integration of such a heterogeneous spectrum of materials on thermally, chemically, and mechanically fragile substrates to build dissolvable thin-film transistors,[10,13,15] sensors,[19] solar cells,[20,21] and batteries.[22–24] The technical

Dr. G. A. Salvatore, J. Sülzle, F. Dalla Valle, G. Cantarella, S. Knobelspies, A. Daus, L. Büthe, L. Petti, Prof. G. Tröster
Electronics Laboratory
ETH Zurich
Gloriastrasse 35, 8092 Zurich, Switzerland
E-mail: giovanni.salvatore@ife.ee.ethz.ch

Dr. F. Robotti
Laboratory of Thermodynamics in Emerging Technologies
ETH Zurich
Sonneggstrasse 3, 8092 Zurich, Switzerland

P. Jokic, Dr. M. Magno
Integrated System Laboratory
ETH Zurich
Gloriastrasse 35, 8092 Zurich, Switzerland

Dr. N. Kirchgessner
Institute of Agricultural Sciences
ETH Zurich
Universitätstrasse 2, 8092 Zürich, Switzerland

Dr. R. Hopf
Institute of Mechanical Systems
ETH Zurich
Leonhardstrasse 21, 8092 Zürich, Switzerland

DOI: 10.1002/adfm.201702390

requirements of such devices may change depending on the specific scenarios. For example, dissolution via hydrolysis is needed in implants while it is not necessary per se in environmental sensing. Thin and soft structures[25,26] have also proven to be greatly beneficial for accurate and precise sensing of biological tissues like skin[27] and inner organs,[28] for textile[29] and food packaging integration[30] or in case of deployment in harsh environments. However, combining good and stable electrical performance with high mechanical deformation and chemical degradation remains still challenging.[31,32] In fact, both mechanical stress and chemical degradation limit the electrical performance (i.e., resolution) and cannot be considered separately when characterizing thin biodegradable sensors. Previous works have reported stretchable and degradable silicon circuits and metal electrodes for electrophysiology.[32] Degradable temperature sensors made of silicon nanomembranes (NMs)[12,19] have also been demonstrated, but not in stretchable format and at the cost of tedious transfer processing of silicon NMs from silicon on insulator donor substrates. The developments of methods and materials which enable simpler and larger area fabrication would be greatly beneficial for application in environmental sensing and internet of things.

This work presents highly deformable resistive temperature sensors that are fully composed by biodegradable materials including magnesium, silicon dioxide and nitride, and a compostable flexible polymer, i.e., Ecoflex by BASF. This polymer is water and tear resistant, optical transparent in the visible spectrum, and possesses a tensile Young's modulus of 500 MPa which, interestingly, approximates that of human muscles and cartilage. Accurate design of the layout allows the sensors to continue to work when completely folded, crumpled, and stretched up to 10% with a resistance variation of about 0.2% K^{-1}. Proper encapsulation with ultrathin Ecoflex films (<20 μm) yields low thermal mass and, consequently, a response time of 10 ms, and tunes the morphological dissolution of the device to 67 d in 1% saline solution while stable electrical operation is lost after about 1 d. The assembly scheme proposed here is scalable as demonstrated by the integration of an array of nine sensors onto an Ecoflex-based fluidic device that provides an example of monolithic, fully biodegradable device for liquid flow mapping. Finally, wireless operation is achieved by connecting the sensors to a Bluetooth module through dissolvable zinc wires. Hardware and software optimization of the wireless node yields a resolution of 200 mK (one standard deviation) and prospects possible application in food tracking.

2. Results and Discussion

2.1. Materials and Design

Figure 1 describes the geometry and the constituent materials of the device. The sensor is formed by three main parts, i.e., the sensing element, the interconnections, and the pads for external wiring. A thin Mg film (250 nm) constitutes the active layer which is sandwiched between two dielectric layers of Si_3N_4 and SiO_2 and two thin films (≈16 μm in total) of Ecoflex acting as substrate and top encapsulation (Figure 1a). Magnesium is biocompatible[33] and dissolvable in water,[17] and is present in the human body, foods, and field fertilizers.[34] Silicon nitride and dioxide have proved to be biocompatible[35,36] and dissolvable in water.[16,17] Ecoflex is a compostable flexible polymer, certified by BASF, blended from corn starch, potato, and polylactic acid.[37,38] Moreover, it is one of the few biodegradable plastics, which complies with its composition with the European (U Directive 2002/72/EC) and American food stuff legislation for food contact (FCN 907). The resistive sensing element consists of 10 μm wide Mg traces (Figure 1b) and its electrical resistance is designed to be 130 times larger than that of the interconnections to minimize the effects of contact resistance and wiring. The interconnections adopt a Peano fractal design[39] to confer stretchability to the whole structure. The total weight of the sensor is less than 0.6 mg cm^{-2}.

Because the minimum resolution of the traces is hard to achieve by a shadow mask, the device is first fabricated on a host template, following steps of UV lithography and etching, and then transfer printed on Ecoflex with the help of a cellulose water soluble tape after etching a Poly(methyl methacrylate), PMMA, sacrificial layer in acetone. During the transfer process, the microstructures are anchored by an additional polyimide layer which is, afterward, removed by reactive ion etching. More details about the fabrication steps are provided in the "Experimental Section" and in Figure S1 of the Supporting Information. Figure 1c shows the final device when bent with hands.

In addition to the curvilinear layout, a stretchable and flexible format is achieved by encapsulating the microstructures with ultra-thin films of Ecoflex. Biodegradable polymers with low Young's modulus are particularly important to interface the soft mechanics of biological tissues, to conformally laminate onto surface without the need of tapes or glues and to accommodate the strain arising from multiaxial deformation. Poly(1,8-octanediol-co-citrate),[40] polycaprolactone,[41] and poly(glycerol sebacate)[42] are some of the materials recently used for tissue engineering,[6] for the encapsulation of skin-like electrodes,[32] and for pressure sensors.[31] Ecoflex is a candidate to complement and enrich this palette[43] considering its easy synthesis and processing, high water and tear resistance, modulus comparable to that of some biological tissues, and small swelling rate (see Table S1 in the Supporting Information for a comparison of various biodegradable elastomers).

In this work, solutions of 5% and 15% concentration (w/v) have been prepared by dissolving the polymer in granular form in chloroform to be further processed by spin coating. While in bulk form, Ecoflex is nontransparent and stiff; when deposited in films thinner than 20 μm, it exhibits an optical transparency greater than 50% in the visible spectrum (Figure 1d). Interestingly, spectrometric measurements reveal a pronounced absorption in the ultraviolet range. Uniaxial tension tests consisting in the application of finite strain (quasistatic stretching) enable the evaluation of the stress from the first Piola–Kirchhoff curve (Figure S2a, Supporting Information). A good estimation of the Young's modulus is computed as a 5% strain secant modulus and yields a value of $E = 533$ MPa which favorably matches that of muscles, tendons, and cartilage.[44] Similarly, the Poisson's ratio is computed from the transverse kinematics (Figure S2b, Supporting Information), which results in a value of $\nu = 0.36$. Figure 1e shows significant wrinkling in the specimen during loading as a consequence of its ultrathin, membrane-like format

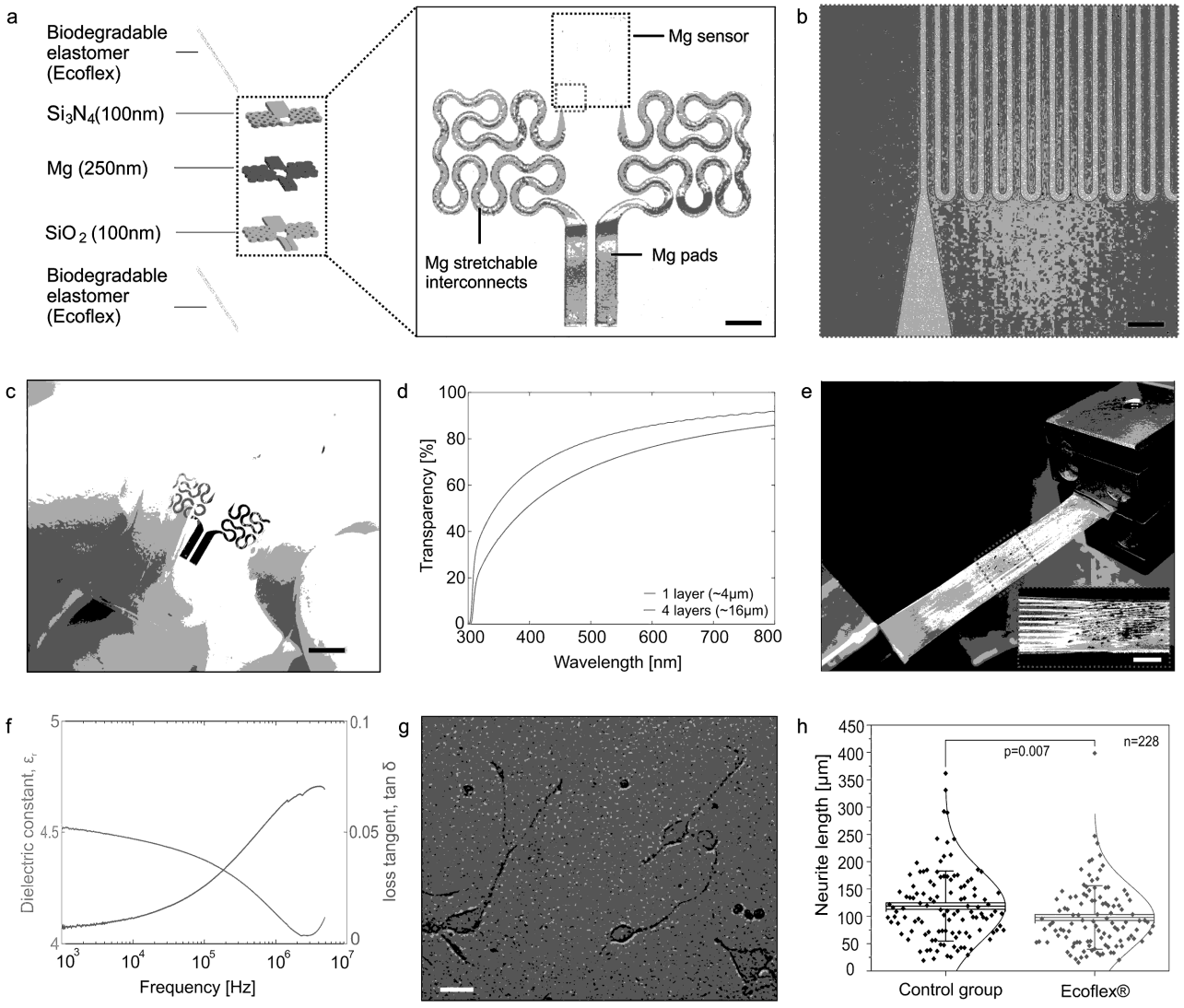

Figure 1. a) The resistive sensor consists of three main parts: the sensing element which is formed by 10 μm wide serpentine traces, Peano-like interconnects, and the pads for contacting and wiring. The active layer is constituted by 250 nm thick Mg deposited by Radio Frequency sputtering. Thin layers of SiN_x, SiO_x, and Ecoflex encapsulate the device and place it in the zero strain plane (scale bar 1 mm). The total weight of the device is less than 10 mg. b) Optical image of the junction area between the serpentine traces forming the sensing element and the interconnects (scale bar 50 μm). c) Optical image of the fully biodegradable sensors during bending experiments (scale bar 1 mm). d) Ecoflex thin films possess an optical transparency higher than 50% in the visible spectrum and show a pronounced absorption in the UV region. e) Stretching tests performed on 1×6 cm^2 stripes of Ecoflex permit to estimate a Young's modulus of about 500 MPa (scale bar 5 mm). The inset shows a zoom view of the Ecoflex film under test and highlights the buckling effect for large loads. f) Ecoflex films with a thickness of ≈800 nm exhibit a dielectric constant of about 4 with associate low leakage at frequency below 5 MHz. g) PC12 neuronal-like cells grown on Ecoflex for cytotoxicity tests. The cells are highlighted in green in the image (scale bar 50 μm). h) After 1 week of incubation, neurite length analysis shows a slightly reduced growth of the cells grown on Ecoflex with respect to a control group. However, no noticeable cell death was detected.

that offers negligible resistance to bending so as to facilitate the buckling.[45] The simulation of a clamped Ecoflex membrane under uniaxial stretching (Figure S3, Supporting Information) and the eigenvalue analysis for structural instabilities confirm the wrinkles formation, which is observed in the experiments.

Electrical characterization of microstructured planar plate capacitors with submicron Ecoflex dielectric layer yields a DC dielectric constant of 4.5, low leakage below 5 MHz (Figure 1f), a normalized capacitance of 4 nF cm^{-2}, and a breakdown field larger than 0.5 MV cm^{-1} (Figure S4, Supporting Information) prospecting its use in low-radio-frequency devices and soft degradable actuators.

The potential interference of Ecoflex with cellular molecular activities, such as cell differentiation, provides relevant information about the cytotoxicity of the material especially important in biomedical applications, environmental sensing and also food packaging. In vitro test consists in the analysis of the neuronal differentiation of PC12 cells seeded on Ecoflex films upon stimulation with nerve growth factor (NGF).[46,47] Chemical stimulation of the neuronal differentiation pathway of PC12

cells initiates a process leading, in a few days, to the generation of cell neurites of several tens of microns. This development can be readily affected by cytotoxic agents causing even small metabolic perturbations of the cells. Figure 1g shows the cells on Ecoflex film after 6 d while Figure 1h reports the average length and the probability density function of the neurites. The neurite length measured for stimulated cells on Ecoflex was generally similar to the values measured on tissue culture plastic (Figure S5, Supporting Information). Nevertheless, a slight, but significant, decrease was detected for cells on Ecoflex. However, PC12 cells on Ecoflex showed the morphology of the cell body and of neurites typical of healthy differentiated cells, indeed very similar to the ones in the control wells. It appears evident that Ecoflex does not impair the differentiation process and does not restrict the metabolic activity of the cells, even if, the small difference in neurite length does not allow excluding categorically a mild cytotoxic effect or, at least, a delay of the differentiation process. The almost complete absence of dead cells also points toward a positive direction, but in vivo tests are necessary to consider the use of Ecoflex in the production of medical and implantable devices.

2.2. Thermal and Mechanical Characterization

Upon completion of the transfer and encapsulation with Ecoflex films, the sensors are calibrated with the help of a hotplate with a 200 mK stability. The sensor exhibits a linear response over a large range of temperature without any hysteretic behavior. The extracted temperature coefficient is 2.45×10^{-3} K^{-1}, which is slightly lower than the reported literature values for thin-film magnesium,[48] and results in an absolute sensitivity of 70 Ω K^{-1} corresponding to a 0.2% K^{-1} relative value (**Figure 2**a). Typical measurements involve the connection to a high precision multimeter (Keysight B2902A) and the averaging of the outputs sampled at 100 Hz with a pulsed voltage of 5 V to yield precision (one standard deviation) of ≈41 mK (see the "Experimental Section" and Figure S6 in the Supporting Information for more details) without any visible self-heating effect (Figure 2b).

The overall thickness of the sensor is less than 20 µm, and such a thin format entails important consequences that go beyond lightness and compliance and impact the thermodynamic and mechanical behavior of the device. One consequence relates to the thermal mass which is about 4.4 mJ cm^{-2} K^{-1}, including the Ecoflex encapsulation, enabling a fast dynamic response (see Table S2 in the Supporting Information for thermal mass calculation). Test experiments, involving the application of a hot droplet of isopropanol on a device suspended in air, reveal a response time smaller than 10 ms (Figure 2c). Similar values have been previously reported for similar nonbiodegradable structures.[27]

Another important consequence of the thin format resides in the sensor response to mechanical stress. The devices continue to work when folded and crumpled with hands with a resistance variation of less than 0.7% (Figure 2d–g). Results from more systematic experiments, involving the bending of the sensors around metallic rods (Figure S7, Supporting Information) with radii as small as 1.75 mm, demonstrate a resistance variation of about 0.06% (Figure 2h). Besides flexibility, the fractal design of the interconnects and the soft mechanics of Ecoflex confer elasticity to the microstructures as demonstrated by the outcomes of stretching tests in both *x*- and *y*-directions (Figure 2i–k; Figure S8, Supporting Information). Accurate and repeated measurements at different strain levels suggest a drift of the resistance which reaches the 0.2% variation at 10% strain without any visible hysteretic effect upon strain release. It is worth mentioning that the devices break upon the application of higher strain levels and that most of the cracks happen at the junction between the pads and the interconnects (Figure 2l).

2.3. Chemical Degradation

Beyond the electrical and mechanical properties, the materials' composition and thickness tune the biochemical degradation. Encapsulation and packaging are, hence, of paramount importance to ensure electrical stability for the desired timeframe and extend the lifetime from minutes to day and weeks. Magnesium traces with a thickness of 250 nm, in fact, dissolve in deionized water and saline solution (150 mmol) at 25 °C in 70 and 18 min (Figure S9, Supporting Information), respectively, which is too fast for any practical applications. In this work, thin Ecoflex films serve both as substrate and top encapsulation (16 µm in total). The latter is achieved by laminating the film on top of the device and heating the sample up to the 120 °C which is the polymer melting temperature (Figure S10, Supporting Information). Among the aforementioned characteristics of Ecoflex, it is also worth mentioning that a swelling rate of about 2.5% measured as a mass change after leaving a $1 \times 1 \times 0.3$ cm^3 sample in water at 25 °C for 24 h. Such a design and a strategy set the morphological dissolution of the SiO_2/Mg/Si_3N_4 structures to 67 d (**Figure 3**a–c) in a 150 mmol saline solution at 25 °C. More importantly, the sensor is able to provide stable and accurate electrical functionalities for about 1 d (Figure 3d), which is sufficient for some applications like food tracking and disposable electronics. Thicker encapsulation layers (SiO_2, Si_3N_4, and Ecoflex) would delay the dissolution at the cost of reduced flexibility.

2.4. Biodegradable Sensors Array for Heat Flow Mapping

The extension of the above-described designs, materials, and assembly schemes from single to sensors array demonstrates the scalability of the approach and broaden the application scenario. Moreover, the properties of Ecoflex, i.e., young modulus, water resistance, and biocompatibility, suggest its use as constituent material for the realization of microfluidic devices. **Figure 4**a and Figure S11 (Supporting Information) describe an array of biodegradable temperature sensors which is integrated onto an Ecoflex-based fluidic device to form a monolithic component for heat flow mapping. The array comprises nine sensors arranged in an octagonal shape and connected by serpentine-like interconnections whose number and complexity are minimized by adopting shared ground signals. The overall array occupies an area of 2.8×2.5 cm^2 (Figure S12, Supporting Information), and all sensors exhibit a linear behavior with a similar

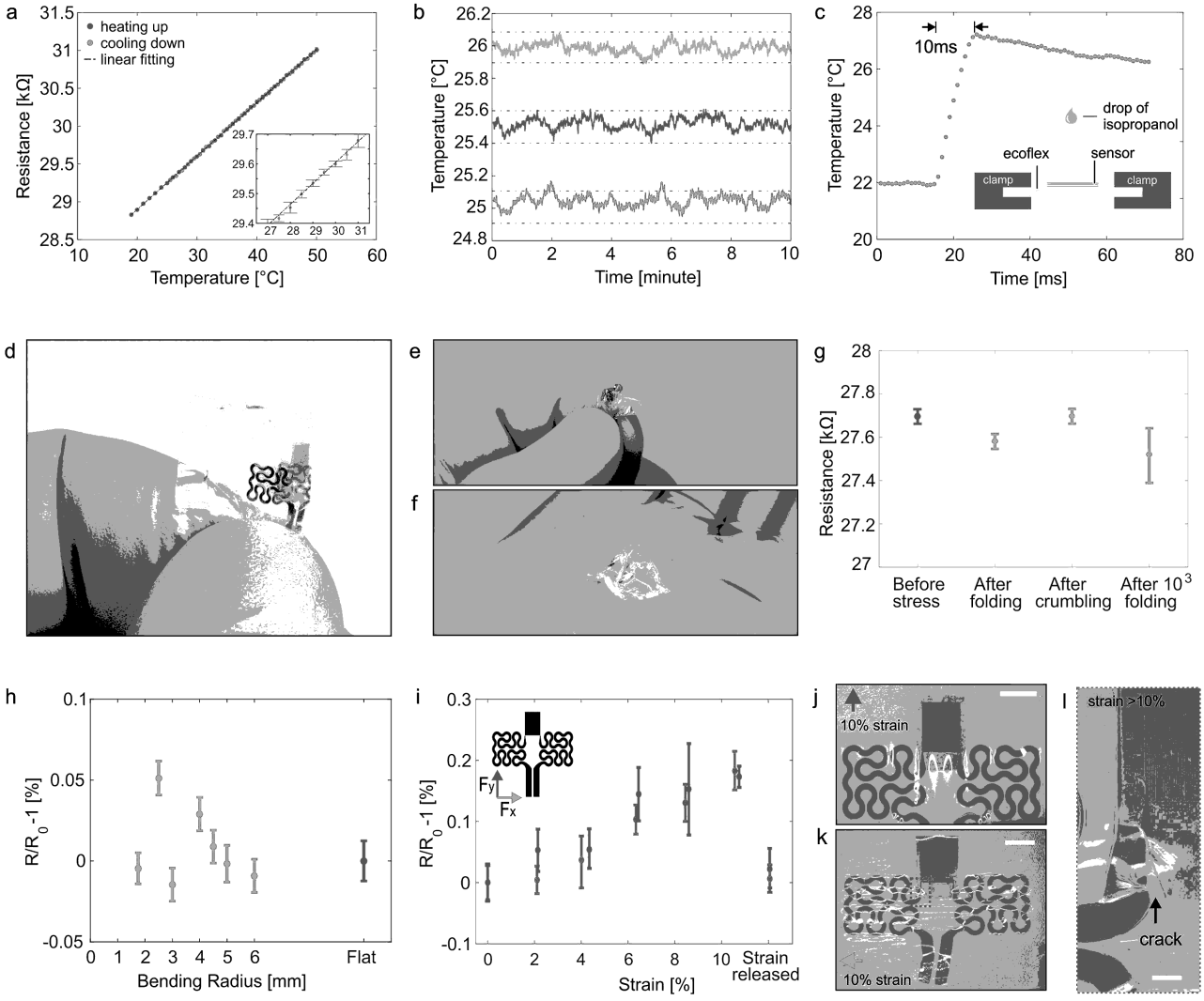

Figure 2. a) The sensor shows a linear response over a wide temperature window with no hysteresis. The change of resistance is about 70 Ω K^{-1} which corresponds to a relative variation of 0.2% K^{-1}. b) The sensor's stability has been tested by measuring the response for 10 min at different temperatures with an acquisition frequency of 100 Hz at 5 V and a duty cycle of 0.04/10 ms. No self-heating effect is registered. The oscillations of the resistance stay in the 0.2 K stability range of the hotplate used in the experiment. c) The sensor has a small thermal capacitance (≈11 mJ cm^{-2} K^{-1}) which enables a dynamic response in the order of 10 ms. The measurement has been performed by releasing a drop of isopropanol onto a sensor suspended between two clamps (inset). d–f) Thanks to its small thickness, the devices continue to work even when folded and crumpled. g) Change of resistance after folding and crumpling the device in hands. The change is less than 0.7% which corresponds to about 3 K. h) More systematical tests consist in bending the devices around rods of various radii. The change in resistance is less than 0.06% for bending radii greater than 1.75 mm. i) The fractal design of the interconnects and the elastic properties of Ecoflex allow to stretch the device in the *x* (blue dots) and *y* (red dots) direction up to 10% with a resistance variation of about 0.2%. j) Optical picture of the device when stretched 10% in the *x* direction (scale bar 1 mm). k) Optical picture of the device when stretched 10% in the *y*-direction (scale bar 1 mm). The wrinkling effect imaged during the mechanical tests of Ecoflex is also visible here. l) The zoom shows a crack occurring for strain larger than 10% at the junction of the interconnections and the resistive element. All mechanical tests have been performed on a set of five devices and error bars represent one standard deviation of the five measurements.

resistive temperature coefficient (Figure S13, Supporting Information). The fluidic device is fabricated by drop casting 15% solution of Ecoflex onto a negative mold made of Teflon and it is sealed with a top Ecoflex layer via thermal heating (see the "Experimental Section" and Figure S14 in the Supporting Information for more details). Typical experiments consist in the injection of a warm liquid (35 °C) into the channels through a programmable syringe pump and the simultaneous monitoring of the sensors' response to map the temperature distribution and flow directions through a digital acquisition system (Figure S15, Supporting Information). Figure 3b proves that the information provided by the biodegradable array spatially and thermally matches that of a handheld infrared camera (FLIR C2). The array of temperature sensors, thanks to low thermal mass, may also be used as a proximity detector as shown in Figure S16 (Supporting Information). Human fingers, when placed at 1 cm distance, generate a temperature change of 2 °C with a dynamic response limited in a few seconds prospecting the possibility for touchless sensing.

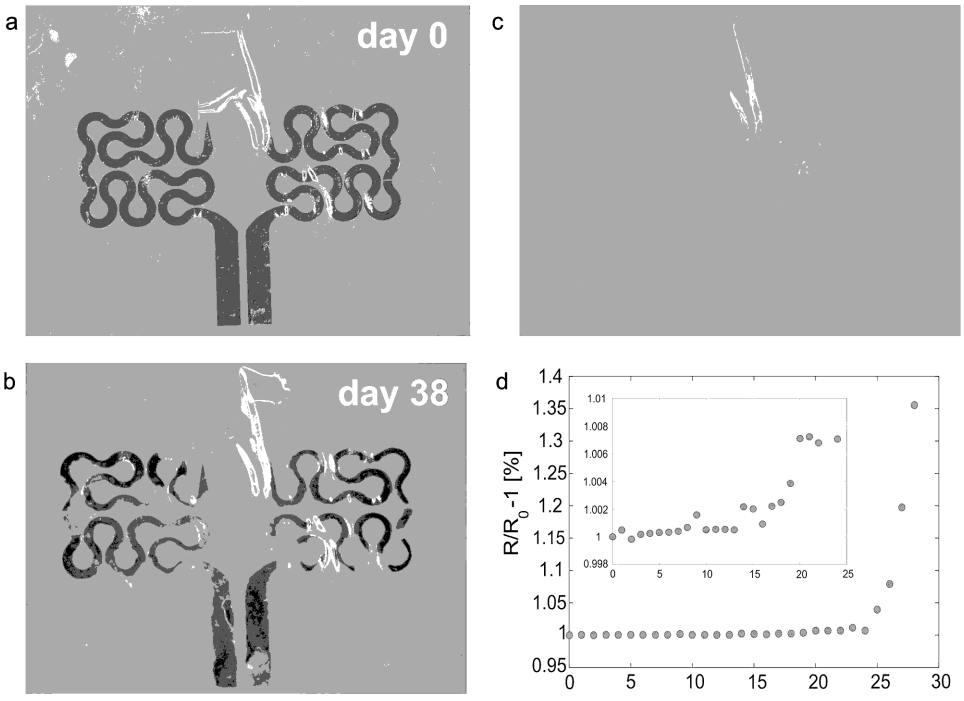

Figure 3. a) Optical image of the sensor before immersion in a water–NaCl solution (150 mmol); b) after 36 d, and c) when completely dissolved after 67 d. Experiments were carried out at 25 °C. d) Continuous measurement of the resistance of the devices while immersed in the water–NaCl solution reveals that the electrical conduction is lost after 30 h. The inset provides a zoom on the first 24 h and shows a resistance variation of 0.6%.

2.5. Wireless Operation

In all previous experiments, the sensor readout has been achieved through high-performance bulky instrumentations including power supplier and high precision multimeters. In practical and real applications, however, it is important to develop wireless and portable designs. Previous relevant work has reported fully degradable passive sensor for pressure monitoring via impedance backscattering scheme.[49] This solution can be effectively applied to capacitive sensors but not to resistive ones, because of the reduced quality factor of the resonant tank. **Figure 5**a shows, instead, a hybrid approach which consists in connecting a high-performance and non-biodegradable electronic circuit board to the biodegradable sensor via degradable Zn wires that are encapsulated with Ecoflex by dip coating. Similar solution has been demonstrated for the monitoring of intracranial pressure,[19] thanks to inductive powering and near-field communication. Here, differently, wireless capabilities are enabled by a low-energy Bluetooth module and a miniaturized Zn–air battery (Figure 5a; Figure S17, Supporting Information) so as to ensure long-term and continuous monitoring. Long measurements prove the stability of the sensor whose output favorably matches that of a conventional thermistor and exhibits a resolution (one standard deviation) which is about 200 mK (Figure 5b). These findings, in combination with the materials compatibility with food contact, suggest possible application in the monitoring of food (Figure 5c). Other possible scenarios are the temperature measurement of hard-to-reach environments and of postsurgery healing processes.

3. Conclusions

This work described the design and fabrication of fully biodegradable temperature sensors whose layout and ultrathin format confer a dynamic response of 10 ms and high mechanical stability, which is preserved even upon application of high strain load. Magnesium was used as an active layer while a commercially available polymer acted as encapsulation, given its easy processing, biocompatibility, small swelling rate, and Young's modulus of 500 MPa. An array of sensors was integrated onto a fluidic device made of the same polymer to yield a smart biodegradable system for flow mapping. Proper encapsulation extended stable electrical operation to 1 d while the connection to a Bluetooth module enables wireless functionalities with 200 mK resolution prospecting application in food tracking and in medical postsurgery monitoring.

4. Experimental Section

4.1 Fabrication, Encapsulation, and Wiring of the Sensors: A standard 4 in. silicon wafer was used as the initial substrate for the fabrication. A thin film of PMMA (AR-P 672.045, 950 K, 4.5% in Anisole, Allresist) was spin-coated at 3000 rpm for 30 s and baked for 1 min at 180 °C. Afterward, polyimide (HD4100, HD MicroSystems) was spin-coated at 5000 rpm for 30 s, baked at 90 °C for 100 s and 100 °C for 100 s, and then hard baked in an oven at 300 °C for 12 h. The resulting thickness of polyimide was about 2 µm. A bottom encapsulation layer was formed by 100 nm of SiO_2, which was deposited by Plasma Enhanced Chemical Vapour Deposition (PECVD) at 120 °C. Magnesium was deposited at room temperature by magnetron sputtering. The thickness of the layer

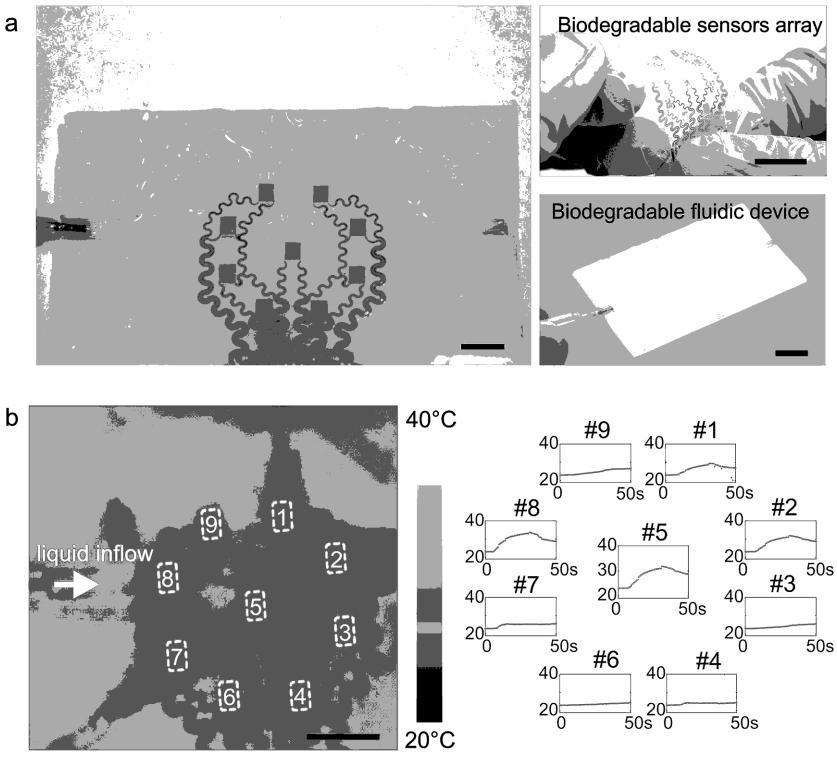

Figure 4. a) Sensors array integrated on top of a biodegradable fluidic device made of Ecoflex. The channels have a width of 3 mm and a height of 1 mm. The fluidic device is fabricated by drop-casting 15% Ecoflex onto a negative Teflon mold and it is sealed with an additional thin Ecoflex layer (scale bar 1 cm). b) The integration of the two devices enables the mapping of hot fluids flowing into the device (scale bar 1 cm). In this case, colored water at 35 °C is injected with the help of a pump connected through a syringe needle. The response of the sensors well matches the information provided by an infrared camera.

was 250 nm. UV lithography defined the structure of the magnesium after the spin coating of AZ1518 resist (MicroChemicals), which was baked at 115 °C for 120 s. The patterns were developed with the developer Microposit (Microresist) for 10–15 s. A solution of HCl with a concentration of 10 mmol L^{-1} was used to etch magnesium for ≈90 s. The patterned magnesium was encapsulated by depositing 100 nm of Si_3N_4 by PECVD at 120 °C, by spin coating another layer of polyimide following the same procedure described previously, and by depositing additional 500 nm of SiO_2 by PECVD at 120 °C. UV lithography defined the final structure of the device. In this case, the resist AZ4620 was spin-coated at 3000 rpm for 30 s, baked before exposure at 110 °C for 240 s, and developed for 75 s in the AZ400K developer (MicroChemicals), diluted 1:3 with DI water. Reactive Ion Etching (RIE) was used to etch the SiO_2/PI/Si_3N_4/SiO_2/PI/PMMA stack. After etching, the samples were clamped between two glass slides which had been wrapped with standard cleanroom wipes. The glasses were placed in an acetone bath overnight to etch the PMMA. After removing from the bath and drying the slides, the samples were removed gently, and the devices were picked with the help of cellulose water soluble tape (Aquasol Corporation). The backside polyimide layer was etched by RIE while the device was still on tape. The devices were then transferred on a glass slide previously spin-coated with a 15% w/v Ecoflex in chloroform solution. Ecoflex was received from BASF in granular form and was stirred overnight in chloroform. The transfer was performed by heating the glass slide with Ecoflex at 130 °C for 2 min and by laminating the device, still stuck to the cellulose tape, on top of it. A gentle pressure was usually applied by fingers or tweezers. The top polyimide layer was finally etched by RIE. The device, with the exception of the contact pads, was encapsulated with another Ecoflex layer which was first laminated on top of the desired area and then heated up to 130 °C for 2 min to melt with the underneath Ecoflex substrate (Figure S2, Supporting Information). The device was wired with Zn (GF40591863-1EA, Sigma Aldrich) or 60 µm thick Cu wires, and silver epoxy (EPO-TEK EJ2189, Epoxy technology) was used as conductive paste in case of wiring. Additional Ecoflex films were used to encapsulate the whole device including the contacts by following the same procedure described previously. Images of the main fabrication steps can be found in the Supporting Information.

4.2 Fabrication of Capacitors and Ecoflex Dielectric Properties Extraction: Capacitors with an active area of 1×1 mm^2 were fabricated on a glass slide which were previously cleaned with acetone and isopropanol. Two layers of Cr/Au (10/50 nm) were deposited by electron beam evaporation and used as the bottom and top electrodes. A 5% solution of Ecoflex was spin-coated at 5500 rpm and cured at 65 °C for 1 min to evaporate the chloroform. The resulting film has a thickness of about 800 nm. The devices were characterized by a semiconductor analyzer (Agilent B1500A). The capacitance–frequency measurement provided the complex impedance of the dielectric. The losses and the real part of the dielectric constant were calculated from the admittance *Y*. The ratio of the real and imaginary parts of *Y* provide information on the dielectric losses

$$\tan(\delta) = \frac{\mathrm{Re}(Y)}{\mathrm{Im}(Y)} \tag{1}$$

Assuming a lumped model of a capacitor in parallel with a resistor, the admittance is formed by the susceptance (*B*) and conductance (*G*)

$$Y = G + jB = G + j\omega \frac{A\varepsilon_0}{t}(\varepsilon_r' - j\varepsilon_r'') \tag{2}$$

where ε_0, *A*, and *t* are, respectively, the vacuum dielectric constant, the area, and the thickness of the capacitors. From Equation (2), the dielectric constant was extracted

$$\varepsilon_r' = \frac{t}{A\varepsilon_0}\frac{\partial B}{\partial \omega} \tag{3}$$

4.3 Fabrication of Biodegradable Fluidic Device: A mold made of Teflon was used as a negative stamp to fabricate the biodegradable fluidic device. A 15% solution of Ecoflex was casted onto the mold and let it cure for 24 h. Shrinking of the specimen dimensions was observed. Afterward, an additional Ecoflex thin film (≈100 µm thick) was spin-coated on a separate glass slide and laminated onto the fluidic devices to seal the channels via thermal heating (130 °C for 2 min). A syringe needle was glued with transparent epoxy at the extremity of one channel and connected to a programmable pump (Syringepump.com).

4.4 Mechanical Tests of Ecoflex: A mechanical characterization of the Ecoflex material was performed for uniaxial stress configuration. The goal was to measure the quasistatic response of Ecoflex for finite strains. For this purpose, thin (of the order of 16 µm) strips of Ecoflex with a length of 60 mm and a width of 10 mm were prepared as test specimens. The final free gauge length was 40 mm after clamping. The test protocol consisted of slow tensile loading with a constant nominal strain rate of 0.25% s^{-1} up to a maximum of 50% nominal strain. The tests were performed on a measurement setup consisting of horizontally mounted hydraulic actuators, 100 N load cells calibrated for a force range of 20 N (MTS Systems, Eden Praire, USA), custom-made clamps, and a Charge-Coupled Device (CCD) camera (Pike F-100B Allied Vision Technologies GmbH, Stadtroda, Germany) equipped with a 0.25× telocentric lens

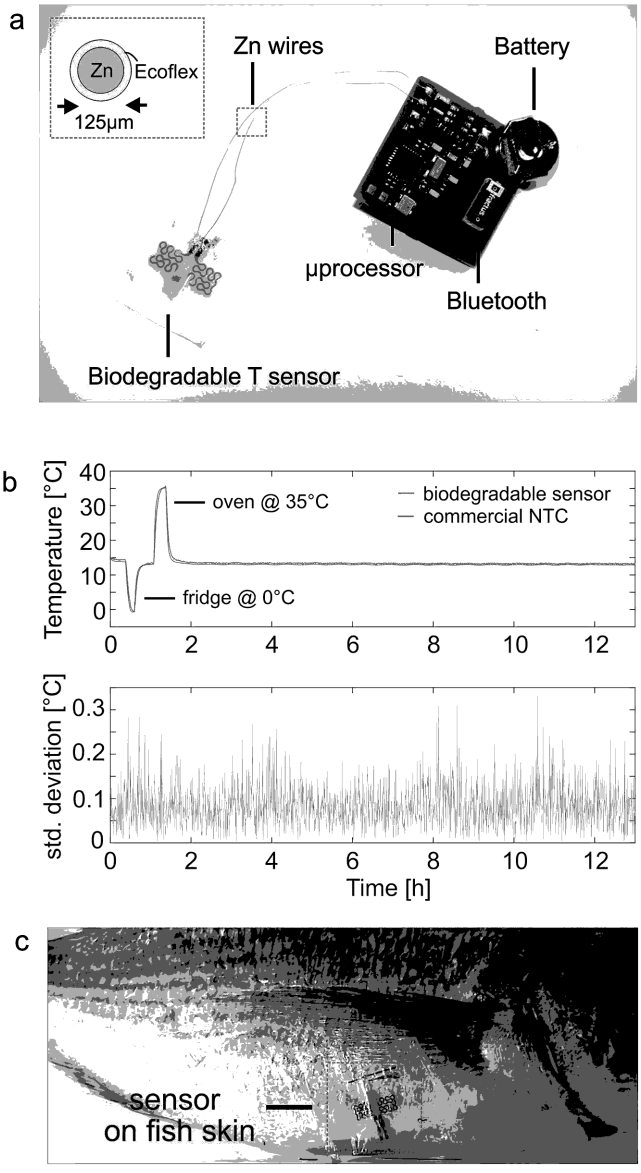

Figure 5. a) Optical image of the sensor connected to a Bluetooth module (scale bar 0.5 cm) through Zn dissolvable wires encapsulated with Ecoflex. b) Temperature measurement in wireless mode for a biodegradable sensor and a conventional Negative Temperature Coefficient (NTC) thermistor (top). The bottom graph illustrates the standard deviation of the measurement for the biodegradable sensor. c) Temperature sensor laminated on top of a fish skin to track its temperature during shipping and storage.

(NT55-349 Edmund Optics GmbH, Karlsruhe, Germany), providing a resolution of 30 µm at a size of 1000 × 1000 pixels per frame. In order to eliminate clamping influences, local material strains were measured optically, by tracking points in the center of the specimen using a Lucas–Kanade-based tracking algorithm. The track points were applied by hand using waterproof ink and a pen. To allow the computation of stresses in the material, the underformed reference cross section of the specimen was determined by measuring the thickness with a profilometer (Dektat). Since these specimens were of very low thickness, wrinkle formation could be observed, especially in the vicinity of clamps. Thus, the local strain measurement was carefully performed in a small, constantly flat region of the center of the specimen to avoid spurious strains due to out-of-plane motions of wrinkling process. Figure 1e shows a clamped Ecoflex specimen and depicts significant wrinkle occurring in the stretched membrane. Since the material is compressible, the strain in thickness direction cannot be computed using a constraint equation from in-plane information. Therefore, the first Piola–Kirchhoff stress measure was chosen, which reported force per reference area (see Figure S2b in the Supporting Information). These data were then used to obtain two small strain material parameters for an isotropic material:[50] Young's modulus and Poisson's ratio.

4.5 Cytotoxicity Tests of Ecoflex: PC12-LA cells were cultured in Roswel Park Memorial Institute (RPMI)-1640 medium supplemented with 10% horse serum, 5% fetal bovine serum (FBS), 2×10^{-3} M L-glutamine, 100 U mL^{-1} penicillin, and 100 µg mL^{-1} streptomycin (all from Sigma-Aldrich, USA). PC12 cells were stably maintained at 37 °C and 5% CO_2. For the cytotoxicity assay, 25 mm glass coverslips (VWR, USA) coated with a layer of Ecoflex were placed into commercial 6-well cell culture plates (TPP, Switzerland), using the tissue culture plastic as control surface. All surfaces were cleaned and activated by oxygen plasma treatment (120 s, 1 mbar) to increase the hydrophilicity and subsequently incubated with 2 mL of poly-L-lysine (PLL) 0.01% solution (Sigma-Aldrich, USA) per well for 30 min at 37 °C. The excess PLL solution was then removed and the wells were rinsed three times with phosphate-buffered saline (5 min each). The well plates were filled with 1.5 mL of induction medium (RPMI medium supplemented with 2% FBS, 2 mmol L-glutamine, 100 U mL^{-1} penicillin and 100 µg mL^{-1} streptomycin) containing neuronal growth factor at a concentration of 100 ng mL^{-1}. Low passage, low adhesion PC12-LA cells were gently detached from subconfluent cultures, and a suspension of single cells was obtained from cells by cyclic pipetting through the 200 µL tip. Cells were counted and re-suspended in the induction medium at a final concentration of 104 cells cm^{-2}. The cells were kept at 37 °C and 5% CO_2 for 6 d, and images were acquired on day 6. Cell images were acquired using an inverted Nikon-Ti wide-field microscope (Nikon, Japan) with an Orca R-2 CCD camera (Hamamatsu Photonics, Japan). An environmentally controlled chamber was used (Life imaging services, Switzerland), where temperature, humidity, and CO_2 concentration were kept at 37 °C, 95%, and 5%, respectively. Images were collected using a 20× magnification, 0.45 numerical aperture long distance air objective (Plan Fluor, Nikon, Japan). For the cytotoxicity experiments, six images at random positions were acquired for each experimental condition. For the analysis of the neurite length in NGF-stimulated PC12 cells, the collected images were loaded into ImageJ (National Institute of Health, USA) and analyzed using the NeuronJ plugin. It is worth mentioning that this test goes beyond simple and conventional methods of detection of early apoptosis and, therefore, gives a deeper insight into the degree of cytotoxicity of a material.

4.6 Device Characterization: A semiconductor analyzer (B1500A, Agilent) and a digital source measure unit (B2902A, Keysight) were used to characterize the single sensors. The former was used for the bending and stretching experiments, while the latter was used for all the other measurements. The digital multimeter was programmed to provide a pulsed signal with a period of 10 ms, a duty cycle of 4%, and an amplitude of 5 V. A single measurement consisted in sampling for 5 s (500 samples) and averaging the results. No self-heating was observed. In case of the measurement of the response time, the sensor was wired and connected to the digital multimeter configured with a sampling frequency of 1 kHz. The calibration was performed by placing the sensor on a hot plate with 200 mK resolution. A thermal paste between the sensor and the plate was used to increase the thermal conductivity while a lid on top of the device reduced the air flow. Concerning the array, a pulsed signal with a period of 10 ms, a duty cycle of 4%, and an amplitude of 5 V was provided to all the sensors with a signal generator (33120A, HP). Each sensor was connected in series with a 30 kΩ resistor. The voltages across the resistive divider were acquired at 10 kHz with a 16-bit Analog Digital Converter (USB-6216, National Instrument) controlled via Labview. Data were averaged over a period of 1 s (300 samples).

4.7 Bending and Stretching Tests: The bending experiments consisted in bending the sensors around metallic rods with the following

radii: 1.75, 3, 4.5, 5, 6, 10 mm. A thin double side tape (3 M) was sometimes used to achieve a more compliant adhesion with the rods. The stretching experiments were performed by mechanical clamping the devices with a custom-made tool (see Figure S8 in the Supporting Information) and by applying unilateral force first in the *x* and, then, in the *y* direction. In both experiments, i.e., in bending and stretching, the resistance was measured with probe tips and a semiconductor analyzer (Agilent B1500A). Multiple measurements (≈20) were recorded, and the results were averaged. Similar procedures were followed for the folding and crumpling experiments. All experiments and measurements were performed on a set of five devices.

4.8 Wireless Sensor Module: The core of the node was a system on chip (CC2650, Texas Instruments) that includes a microcontroller ARM Cortex M3, on board memory, and wireless capability trough an ARM Cortex M0 Bluetooth low-energy (BTLE) subsystem. The chip guarantees enough computational power to acquire and process the data (EEMBC CoreMark Score: 142) combined with low power consumption (≈61 μA MHz^{-1}). A general purpose input/output is used to supply the voltage to an in-series resistive divider (30 kΩ resistor + biodegradable sensor) and the potential on the biodegradable sensor acquired through the internal 12-bit analog digital converter. The chip sampled and streamed the data via the BTLE subsystem which was connected to a chip antenna (FR05-S1, Fractures Antenna) able to provide a gain of +1.1 dBi in a small form factor (7.0 mm × 3.0 mm). The powering was happened through a coin zinc–air battery (Activair 312, Duracell), which had a diameter of 7.9 mm and provided 180 mAh at 1.45 V (nominal in an open circuit). As the CC2650 system on chip required a voltage of at least 1.8 V to work properly, a DC-to-DC converter (TPS61072, Texas Instrument) was needed to boost up the voltage of the battery to 1.8 V. The wireless tests were conducted by connecting the biodegradable sensors to the node through dissolvable zinc wires (GF40591863-1EA, Sigma Aldrich) and by acquiring and streaming the data to a Bluetooth receiver (Launchxl-CC2650, Texas Instruments) for each 30 s. For proof-of-concept demonstration, conductive silver epoxy (EPO-TEK EJ2189, Epoxy technology) was used to connect the sensor to the wireless board, but degradable tungsten-based conductive paste was reported previously.[51] In the remaining time, the node was set to sleeping mode to reduce power consumption and not to cause self-heating. A single acquisition consisted of 160 samples. Experiments demonstrated the node streams data at a 20 m distance with a power consumption of 41 μW (averaged consumption over 30 s). A second wireless node with a conventional 10 kΩ thermistor (ncp15xh103f03rc, Murata) connected to a second Bluetooth receiver was used as a reference in the measurement as shown in Figure 5c.

Supporting Information

Supporting Information is available from the Wiley Online Library or from the author.

Acknowledgements

F.R. was supported by the CINDY project, supported by the Swiss National Science Foundation (SNSF 2-77795-13). F.D.V. was supported by the Swiss-European mobility program. S.K. is supported by a grant from the Schweizer Nationalfond (SNF), Switzerland, through the project "WISDOM: Wireless Indium–Gallium–Zinc–Oxide Transmitters and Devices on Mechanically Flexible Thin-Film Substrates" (Grant No. 200021E-160347/1). The authors thank Dr. Mauro Ciappa for the help and hints on the thermal characterization. The first lab team at ETH Zurich deserves a special mention for the support in the fabrication process. Mr. Martin Vogt from the D-ITET mechanical workshop is acknowledged for the fabrication of the Teflon mold for the fluidic device. Many thanks go to Mr. Gabriel Skupin at BASF for providing the Ecoflex material.

Conflict of Interest

The authors declare no conflict of interest.

Keywords

biodegradable materials, electronics, flexible sensors, sensors, stretchable sensors

Received: May 4, 2017
Published online:

[1] V. Siracusa, P. Rocculi, S. Romani, M. Dalla Rosa, *Trends Food Sci. Technol.* **2008**, *19*, 634.
[2] R. A. Gross, B. Kalra, *Science* **2002**, *297*, 803.
[3] M. Avella, J. J. De Vlieger, M. E. Errico, S. Fischer, P. Vacca, M. G. Volpe, *Food Chem.* **2005**, *93*, 467.
[4] B. Amsden, *Soft Matter* **2007**, *3*, 1335.
[5] B. Jeong, Y. H. Bae, D. S. Lee, S. W. Kim, *Nature* **1997**, *388*, 860.
[6] J. Yang, A. R. Webb, G. A. Ameer, *Adv. Mater.* **2004**, *16*, 511.
[7] K. R. King, C. C. J. Wang, M. R. Kaazempur-Mofrad, J. P. Vacanti, J. T. Borenstein, *Adv. Mater.* **2004**, *16*, 2007.
[8] A. Datta, S. T. Huxel, D. D. Jamiolkowski, Y. Li, *U.S. Patent No. 6338739*, **2002**.
[9] J. C. Middleton, A. J. Tipton, *Biomaterials* **2000**, *21*, 2335.
[10] C. J. Bettinger, Z. Bao, *Adv. Mater.* **2010**, *22*, 651.
[11] M. Irimia-Vladu, P. A. Troshin, M. Reisinger, L. Shmygleva, Y. Kanbur, G. Schwabegger, M. Bodea, R. Schwödiauer, A. Mumyatov, J. W. Fergus, *Adv. Funct. Mater.* **2010**, *20*, 4069.
[12] S.-W. Hwang, H. Tao, D.-H. Kim, H. Cheng, J.-K. Song, E. Rill, M. A. Brenckle, B. Panilaitis, S. M. Won, Y.-S. Kim, *Science* **2012**, *337*, 1640.
[13] C. Dagdeviren, S.-W. Hwang, Y. Su, S. Kim, H. Cheng, O. Gur, R. Haney, F. G. Omenetto, Y. Huang, J. A. Rogers, *Small* **2013**, *9*, 3398.
[14] S. H. Jin, S.-K. Kang, I.-T. Cho, S. Y. Han, H. U. Chung, D. J. Lee, J. M. Shin, G. W. Baek, T.-I. Kim, J. Lee, *ACS Appl. Mater. Interfaces* **2015**, *7*, 8268.
[15] M. Irimia-Vladu, E. D. Głowacki, G. Voss, S. Bauer, N. S. Sariciftci, *Mater. Today* **2012**, *15*, 340.
[16] S.-K. Kang, S.-W. Hwang, H. Cheng, S. Yu, B. H. Kim, J.-H. Kim, Y. Huang, J. A. Rogers, *Adv. Funct. Mater.* **2014**, *24*, 4427.
[17] L. Yin, H. Cheng, S. Mao, R. Haasch, Y. Liu, X. Xie, S.-W. Hwang, H. Jain, S.-K. Kang, Y. Su, R. Li, Y. Huang, J. A. Rogers, *Adv. Funct. Mater.* **2014**, *24*, 645.
[18] Y. H. Jung, T.-H. Chang, H. Zhang, C. Yao, Q. Zheng, V. W. Yang, H. Mi, M. Kim, S. J. Cho, D.-W. Park, H. Jiang, J. Lee, Y. Qiu, W. Zhou, Z. Cai, S. Gong, Z. Ma, *Nat. Commun.* **2015**, *6*, 7170.
[19] S.-K. Kang, R. K. J. Murphy, S.-W. Hwang, S. M. Lee, D. V. Harburg, N. A. Krueger, J. Shin, P. Gamble, H. Cheng, S. Yu, Z. Liu, J. G. McCall, M. Stephen, H. Ying, J. Kim, G. Park, R. C. Webb, C. H. Lee, S. Chung, D. S. Wie, A. D. Gujar, B. Vemulapalli, A. H. Kim, K.-M. Lee, J. Cheng, Y. Huang, S. H. Lee, P. V. Braun, W. Z. Ray, J. A. Rogers, *Nature* **2016**, *530*, 71.
[20] Y. Zhou, C. Fuentes-Hernandez, T. M. Khan, J.-C. Liu, J. Hsu, J. W. Shim, A. Dindar, J. P. Youngblood, R. J. Moon, B. Kippelen, *Sci. Rep.* **2013**, *3*, 1536.
[21] M. Strange, D. Plackett, M. Kaasgaard, F. C. Krebs, *Sol. Energy Mater. Sol. Cells* **2008**, *92*, 805.
[22] X. Jia, C. Wang, C. Zhao, Y. Ge, G. G. Wallace, *Adv. Funct. Mater.* **2016**, *26*, 1454.
[23] K. Fu, Z. Liu, Y. Yao, Z. Wang, B. Zhao, W. Luo, J. Dai, S. D. Lacey, L. Zhou, F. Shen, M. Kim, L. Swafford, L. Sengupta, L. Hu, *Nano Lett.* **2015**, *15*, 4664.

[24] M. Tsang, A. Armutlulu, A. W. Martinez, S. A. B. Allen, M. G. Allen, *Microsyst. Nanoeng.* **2015**, *1*, 15024.
[25] M. Kaltenbrunner, T. Sekitani, J. Reeder, T. Yokota, K. Kuribara, T. Tokuhara, M. Drack, R. Schwodiauer, I. Graz, S. Bauer-Gogonea, S. Bauer, T. Someya, *Nature* **2013**, *499*, 458.
[26] G. A. Salvatore, N. Münzenrieder, T. Kinkeldei, L. Petti, C. Zysset, I. Strebel, L. Büthe, G. Tröster, *Nat. Commun.* **2014**, *5*, 2982.
[27] R. C. Webb, A. P. Bonifas, A. Behnaz, Y. Zhang, K. J. Yu, H. Cheng, M. Shi, Z. Bian, Z. Liu, Y.-S. Kim, W.-H. Yeo, J. S. Park, J. Song, Y. Li, Y. Huang, A. M. Gorbach, J. A. Rogers, *Nat. Mater.* **2013**, *12*, 938.
[28] L. Xu, S. R. Gutbrod, A. P. Bonifas, Y. Su, M. S. Sulkin, N. Lu, H.-J. Chung, K.-I. Jang, Z. Liu, M. Ying, C. Lu, R. C. Webb, J.-S. Kim, J. I. Laughner, H. Cheng, Y. Liu, A. Ameen, J.-W. Jeong, G.-T. Kim, Y. Huang, I. R. Efimov, J. A. Rogers, *Nat. Commun.* **2014**, *5*, 3329.
[29] C. Zysset, N. Nasseri, L. Büthe, N. Münzenrieder, T. Kinkeldei, L. Petti, S. Kleiser, G. A. Salvatore, M. Wolf, G. Tröster, *Opt. Exp.* **2013**, *21*, 3213.
[30] K. Marsh, B. Bugusu, *J. Food Sci.* **2007**, *72*, R39.
[31] C. M. Boutry, A. Nguyen, Q. O. Lawal, A. Chortos, S. Rondeau-Gagné, Z. Bao, *Adv. Mater.* **2015**, *27*, 6954.
[32] S.-W. Hwang, C. H. Lee, H. Cheng, J.-W. Jeong, S.-K. Kang, J.-H. Kim, J. Shin, J. Yang, Z. Liu, G. A. Ameer, *Nano Lett.* **2015**, *15*, 2801.
[33] G. Song, *Corros. Sci.* **2007**, *49*, 1696.
[34] *U. S. A. National Institute of Health*, https://ods.od.nih.gov/factsheets/Magnesium-HealthProfessional/ (accessed: 2016).
[35] A. Neumann, T. Reske, M. Held, K. Jahnke, C. Ragoss, H. Maier, *J. Mater. Sci.: Mater. Med.* **2004**, *15*, 1135.
[36] G. Voskerician, M. S. Shive, R. S. Shawgo, H. Von Recum, J. M. Anderson, M. J. Cima, R. Langer, *Biomaterials* **2003**, *24*, 1959.
[37] *BASF Product Information*, http://product-finder.basf.com/group/corporate/product-finder/en/literature-document:/Brand+ecoflex-Product+Data+Sheet--Ecoflex+F+Blend+C1200-English.pdf (accessed: 2013).
[38] M. Irimia-Vladu, P. A. Troshin, M. Reisinger, G. Schwabegger, M. Ullah, R. Schwoediauer, A. Mumyatov, M. Bodea, J. W. Fergus, V. F. Razumov, *Org. Electron.* **2010**, *11*, 1974.
[39] J. A. Fan, W.-H. Yeo, Y. Su, Y. Hattori, W. Lee, S.-Y. Jung, Y. Zhang, Z. Liu, H. Cheng, L. Falgout, M. Bajema, T. Coleman, D. Gregoire, R. J. Larsen, Y. Huang, J. A. Rogers, *Nat. Commun.* **2014**, *5*, 3266.
[40] J. Yang, A. R. Webb, S. J. Pickerill, G. Hageman, G. A. Ameer, *Biomaterials* **2006**, *27*, 1889.
[41] M. A. Woodruff, D. W. Hutmacher, *Prog. Polym. Sci.* **2010**, *35*, 1217.
[42] Y. Wang, G. A. Ameer, B. J. Sheppard, R. Langer, *Nat. Biotechnol.* **2002**, *20*, 602.
[43] M. C. Serrano, E. J. Chung, G. Ameer, *Adv. Funct. Mater.* **2010**, *20*, 192.
[44] C. T. McKee, J. A. Last, P. Russell, C. J. Murphy, *Tissue Eng., Part B* **2011**, *17*, 155.
[45] V. Nayyar, K. Ravi-Chandar, R. Huang, *Int. J. Solids Struct.* **2011**, *48*, 3471.
[46] T. Vasileiou, D. Foresti, A. Bayram, D. Poulikakos, A. Ferrari, *Sci. Rep.* **2016**, *6*.
[47] A. Ferrari, M. Cecchini, M. Serresi, P. Faraci, D. Pisignano, F. Beltram, *Biomaterials* **2010**, *31*, 4682.
[48] P. Renucci, L. Gaudart, J. Petrakian, D. Roux, *Thin Solid Films* **1985**, *130*, 75.
[49] M. Luo, A. W. Martinez, C. Song, F. Herrault, M. G. Allen, *J. Microelectromech. Syst.* **2014**, *23*, 4.
[50] R. Hopf, L. Bernardi, J. Menze, M. Zündel, E. Mazza, A. Ehret, *J. Mech. Behav. Biomed. Mater.* **2016**, *60*, 425.
[51] X. Huang, Y. Liu, S. W. Hwang, S. K. Kang, D. Patnaik, J. F. Cortes, J. A. Rogers, *Adv. Mater.* **2014**, *26*, 7371.